Editors' Suggestion

Cell Sorting in an Active Nematic Vertex Model

Jan Rozman* and Julia M. Yeomans
Rudolf Peierls Centre for Theoretical Physics, University of Oxford, Oxford OX1 3PU, United Kingdom

(Received 7 August 2024; accepted 18 November 2024; published 10 December 2024)

We study a mixture of extensile and contractile cells using a vertex model extended to include active nematic stresses. The two cell populations phase separate over time. While phase separation strengthens monotonically with an increasing magnitude of contractile activity, the dependence on extensile activity is nonmonotonic, so that sufficiently high values reduce the extent of sorting. We interpret this by showing that extensile activity renders the system motile, enabling cells to undergo neighbor exchanges. Contractile cells that come into contact as a result are then more likely to stay connected due to an effective attraction arising from contractile activity.

DOI: 10.1103/PhysRevLett.133.248401

Introduction—Phase separation in biological systems plays a role on scales ranging from mixtures of RNA and charged proteins [1] to populations of cells [2]. In particular, cell sorting has been observed, e.g., in *in vitro* mixtures of cell from different tissues [3,4] and hydra regeneration [5,6]. It is suggested to underpin the formation of boundaries between regions of different cells in developmental contexts [2,7] and has been implicated in the organization of tumors [8]. Therefore, the mechanisms behind it have long been of interest. In an important step Steinberg proposed the differential adhesion hypothesis to explain cell sorting, suggesting that it arises from differences in adhesion between like and unlike cell types [9,10]. However, biological systems are active [11,12], allowing for sorting not driven by equilibrium energy minimization. The most well known active phase separation mechanism is the motility-induced phase separation [13–15] of self-propelled particles forming a dense and a dilute phase.

Active nematics are a type of active matter characterized by components generating dipolar stresses, resulting in chaotic flows termed active turbulence [16,17]. They have been used to model, e.g., Madin-Darby canine kidney (MDCK) cells, a type of epithelium [18], fibroblasts [19,20], and bacterial colonies [21]. Of particular relevance to this Letter, Ref. [22] reports that wild type MDCK cells resemble extensile active nematics, whereas E-cadherin knockout MDCK cells resemble contractile active nematics. In a mixture of wild type (extensile) and E-cadherin knockout (contractile) MDCK cells, the two populations phase separate. Phase separation in mixtures of active nematics with different activities has also been demonstrated in theoretical models [22–25].

2D vertex models, which represent epithelial cells as polygons tiling a surface, are a powerful tool for understanding tissue mechanics [26–29]. Examples of phase separation mechanisms in vertex models are the interplay of local alignment and contact inhibition of locomotion in polar models which produces phase separation in cell density [30], as well as different amplitudes of fluctuating tensions on cell-cell junctions [31] and, on small scales, differences in cell shape [32] which lead to cell sorting. Recent work has shown that it is possible to generalize vertex models to include active nematic driving [33–38]. Therefore, given the relevance of nematic activity to tissue dynamics, we investigate cell sorting in an active nematic vertex model. We find that a mixture of extensile and contractile cells (i.e., cells where the active stresses tend to either extend or to contract them along their long axis) phase separates over time, with two mechanisms contributing to the separation: (i) the motility of the extensile cells and (ii) contractile activity causing an effective attraction between contractile cells.

The model—We use the area and perimeter elasticity vertex model [27] extended to include nematic activity [35,36]. The dimensionless energy function is $e_{\mathrm{VM}} = (1/2)\sum_i[(a_i-1)^2 + k_{\mathrm{P}}(p_i-p_0)^2]$. Here, the sum is over all N_{c} cells, a_i is the area of cell i, k_{P} is the perimeter elasticity modulus, p_i is the perimeter of cell i, and p_0 is the target perimeter. p_0 determines the mechanical properties of the passive model, controlling its rigidity transition at a critical value p_*, which was first reported at 3.81 [39]. Further studies place the rigidity transition threshold value of the purely passive vertex model in the range ≈3.81–3.94 [40–42].

Dynamics are given by the overdamped equation of motion, which reads in dimensionless form: $\dot{\mathbf{r}}_j = -\nabla_{\mathbf{r}_j} e_{\mathrm{VM}} + \mathbf{f}_j^{\mathrm{act}}$, where $\mathbf{r}_j$ is the position of vertex j, the

*Contact author: jan.rozman@physics.ox.ac.uk

overdot indicates the time derivative, $\nabla_{\mathbf{r}_j}$ is the gradient with respect to the position of vertex j, and $\mathbf{f}_j^{\mathrm{act}}$ is the active force on vertex j. We define the active nematic forces following Ref. [36]. Each cell i experiences a bulk stress

$$\boldsymbol{\sigma}_i = -\zeta_i \mathbf{Q}_i, \tag{1}$$

where ζ_i is the activity of the cell and $\mathbf{Q}_i = [(1/p_i)\sum_k \ell_k \hat{\mathbf{t}}_k \otimes \hat{\mathbf{t}}_k] - \frac{1}{2}\mathbf{I}$ is a cell shape anisotropy tensor. The sum is along all junctions k of cell i, ℓ_k is the length of junction k, $\hat{\mathbf{t}}_k$ a unit vector along the direction of the junction, and $\mathbf{I}$ is the identity tensor. The stress tensor is converted into vertex forces using the approach proposed by Tlili *et al.* [43,44] (see Supplemental Material, Sec. I [45]). Positive values of ζ correspond to extensile activity, whereas negative values correspond to contractile activity. In the case where all cells have the same extensile activity ($\zeta_i = \zeta_e > 0$) and the activity is above a threshold (which falls to 0 for $p_0 > p_*$), this model has been shown to produce chaotic flows resembling extensile active nematic turbulence [36].

We solve the equations of motion using a simple Euler scheme with time step $\Delta t = 0.01$. If the length of a junction falls below a threshold $\ell_{\mathrm{T1}} = 0.01$, a T1 transition is performed, with final junction length set to $\ell'_{\mathrm{T1}} = 1.1 \times \ell_{\mathrm{T1}}$ (Fig. S1; see Supplemental Material, Sec. II [45], for discussion on how ℓ_{T1} and ℓ'_{T1} affect simulation results). Unless otherwise specified, we set $k_{\mathrm{P}} = 0.02$ and $p_0 = 3.95$, corresponding to the fluid phase of the passive vertex model. We use a system of 1024 cells with periodic boundary conditions. The initial configuration is a 32 by 32 cell hexagonal lattice, with all vertices displaced by a small random perturbation so that cells start with a finite $\mathbf{Q}_i$ tensor. Without the perturbation, all components of $\mathbf{Q}_i$ would be 0 for a regular hexagon, resulting in no active forces at the start of the simulation. Simulations are run until $t = 6 \times 10^5$ unless otherwise specified.

Results—We begin by simulating a model tissue in which half of the cells are randomly selected to be extensile ($\zeta_i = \zeta_e$), whereas the remainder are contractile ($\zeta_i = \zeta_c$). The initial configuration is shown in Fig. 1(a). The extensile and contractile cells phase separate over time [Fig. 1(b) and Movie S1]. To quantify the extent of phase

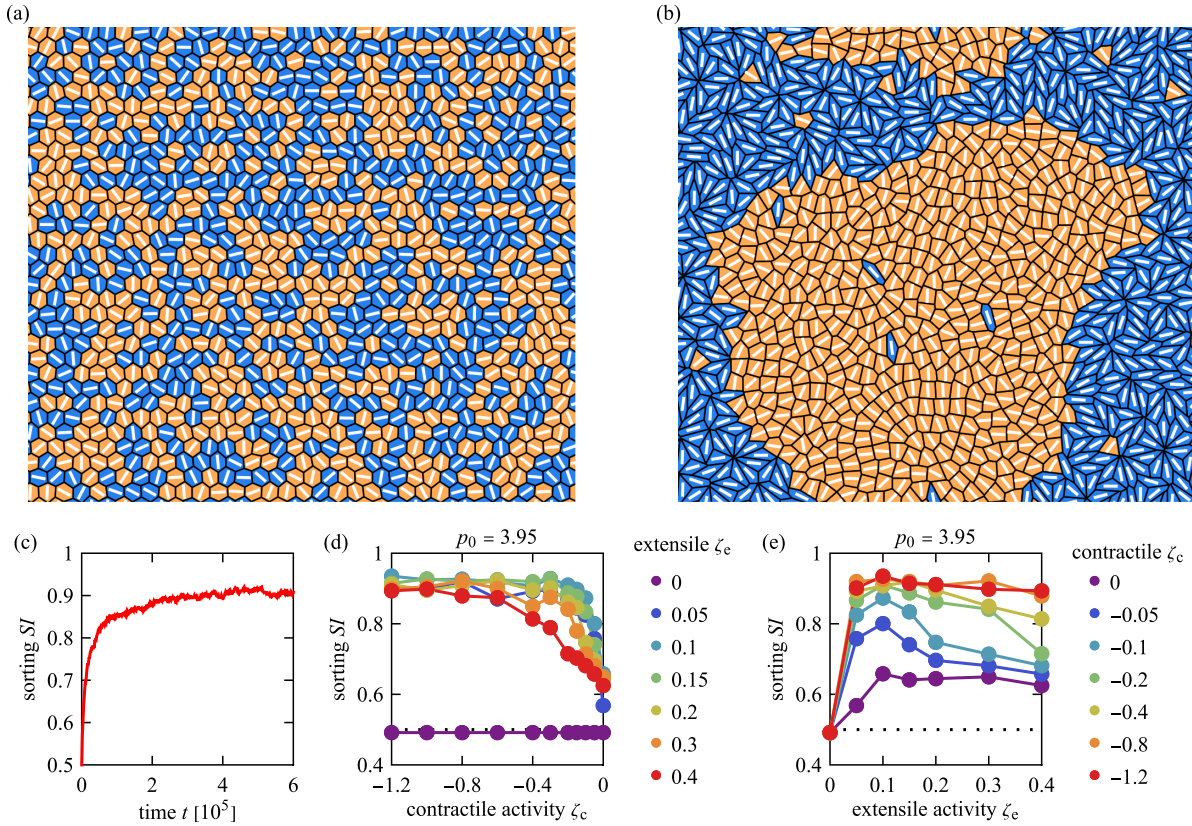

FIG. 1. (a) Initial condition of the simulation: blue cells are extensile ($\zeta_e = 0.1$) and orange cells are contractile ($\zeta_c = -0.4$). White lines show cell directors. (b) Model tissue at $t = 6 \times 10^5$, showing phase separation between the extensile and contractile cells. (c) Segregation index SI as a function of time for the simulation shown on panels (a),(b). (d),(e) Segregation index at $t = 6 \times 10^5$ as a function of contractile activity at different extensile activities (d) and as a function of extensile activity at different contractile activities (e). Dotted lines on panels (d) and (e) show $SI = 0.5$. $k_{\mathrm{P}} = 0.02$ and $p_0 = 3.95$ for all panels.

separation, we use the segregation index $SI = (1/N_c)\sum_{i=1}^{N_c}[n_i/(n_i + n_i')]$ [24,50], where n_i is the number of neighbors of cell i that are of the same type and n_i' is the number of neighbors of a different type. Figure 1(c) shows how the SI changes over time for $\zeta_e = 0.1$ and $\zeta_c = -0.4$. While the speed of the sorting slows down over time, almost all extensile cells form a single contiguous region by the end of the simulation [Fig. 1(b)]. The same is also true for the contractile cells.

Scanning over extensile and contractile activities, we find that the SI at the end of the simulation depends monotonically on ζ_c so that a higher magnitude of contractile activity results in better (or equal) phase separation [Fig. 1(d)]. However, although extensile activity is required for phase separation, the SI depends on it nonmonotonically. Increasing ζ_e above an optimal value reduces sorting [Fig. 1(e)].

The sorting remains similar at $p_0 = 3.85$, closer to the originally reported threshold of the passive vertex model rigidity transition $p_* = 3.81$ [39] (Fig. S2). Moreover, the extensile-contractile mixture still separates if p_0 is below p_* (Fig. S3 [45]): the dependence on contractile activity remains monotonic and the dependence on extensile activity nonmonotonic. However, as shown in Ref. [36], extensile activity must be above a threshold value to fluidize the tissue if $p_0 < p_*$, whereas any extensile activity should fluidize it above p_* [see Fig. 3(e) in Ref. [36] for the phase diagram]. Correspondingly, sorting only takes place if ζ_e is sufficiently high, approximately matching the reported value for active tissue fluidization. Moreover, an extensile-passive or extensile-extensile mixture also features some phase separation, whereas a contractile-passive or contractile-contractile one does not (Fig. S4 [45]).

To understand the mechanisms behind phase separation, we first measure cell motility in the model using the mean-squared displacement of cells $\mathrm{MSD}(t) = (1/N_c)\sum_{i=1}^{N_c}|\mathbf{r}_i^{(c)}(t) - \mathbf{r}_i^{(c)}(t_0)|^2$. Here, N_c is the total cell number, $\mathbf{r}_i^{(c)}(t)$ is the position of the center (mean of vertices) of cell i at time t, and $t_0 = 3 \times 10^5$ is the starting time for MSD measurements. Only extensile activity is reported to result in the system behaving as a motile active fluid (provided activity is above a threshold if $p_0 < p_*$) [36]. As expected, cells in a purely extensile system move diffusively and are much more motile than cells in a purely contractile system [Fig. 2(a)]. In a mixture, contractile cells become more motile but still move less than their extensile counterparts [Fig. 2(b)]. Phase separation due to differential diffusivity is a known mechanism [51,52] and it has been suggested to drive extensile-contractile phase separation in an active nematic phase-field model [24]. However, Ref. [52] reports that differential diffusivity does not induce phase separation at high packing fractions in a particle-based or a Voronoi model. The latter is closely related to the vertex model, and both represent confluent tissues,

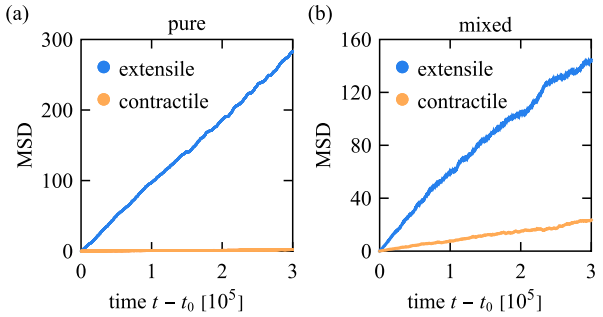

FIG. 2. (a) Mean-squared displacement (MSD) of a system of only extensile ($\zeta_e = 0.1$) or only contractile ($\zeta_c = -0.4$) cells. (b) MSD of a 50:50 mixture of extensile ($\zeta_e = 0.1$) and contractile ($\zeta_c = -0.4$) cells. $k_P = 0.02$ and $p_0 = 3.95$ for both panels.

corresponding to packing fraction one. This suggests that other mechanisms are necessary to cause the cell sorting observed here.

Therefore, to further investigate why phase separation takes place, we simulate a small, 64 cell, contractile cluster in an extensile bulk until $t = 10^5$ [Fig. 3(a)]. First selecting $\zeta_c = -0.1$ for the cluster and $\zeta_e = 0.1$ for the bulk, we find that the majority of the contractile cells remain connected over time. However, if extensile activity is increased to $\zeta_e = 0.4$, the cluster no longer remains connected and its largest component at $t = 5 \times 10^4$ only has a few cells. Conversely, keeping the higher extensile activity $\zeta_e = 0.4$ and increasing the magnitude of the contractile activity to $\zeta_c = -0.8$ improves the stability of the cluster. This shows that while a higher extensile activity aids in breaking the cluster apart, a higher magnitude of contractile activity holds the cluster together better, suggesting an effective attraction between contractile cells. This is also supported by Figs. 3(b) and 3(c), which show how the average size of the largest cluster of connected contractile cells changes over time for different extensile and contractile activities, as well as Fig. 3(d), which shows the size of the largest cluster at the end of the simulation ($t = 10^5$) for different ζ_e and ζ_c.

As evidence that the effective attraction is intrinsic to the contractile cells and does not depend on the presence of an extensile bulk, we simulate an alternative model in which the contractile cluster is surrounded by passive cells, but each contractile cell also experiences a polar force [46] pointing in a constant random direction (see Supplemental Material, Sec. III [45], for details). Increasing contractile activity again improves the stability of the cluster (Fig. S5 [45]). A plausible reason for the effective attraction is that, as shown in Ref. [36], the contractile activity considered here increases the shear modulus of the tissue, rendering a vertex model solidlike even above the passive rigidity transition threshold. Therefore, a connected contractile region should oppose deformation and, as a consequence, resist being separated into smaller regions. To quantify the effective attraction, we measure the threshold force

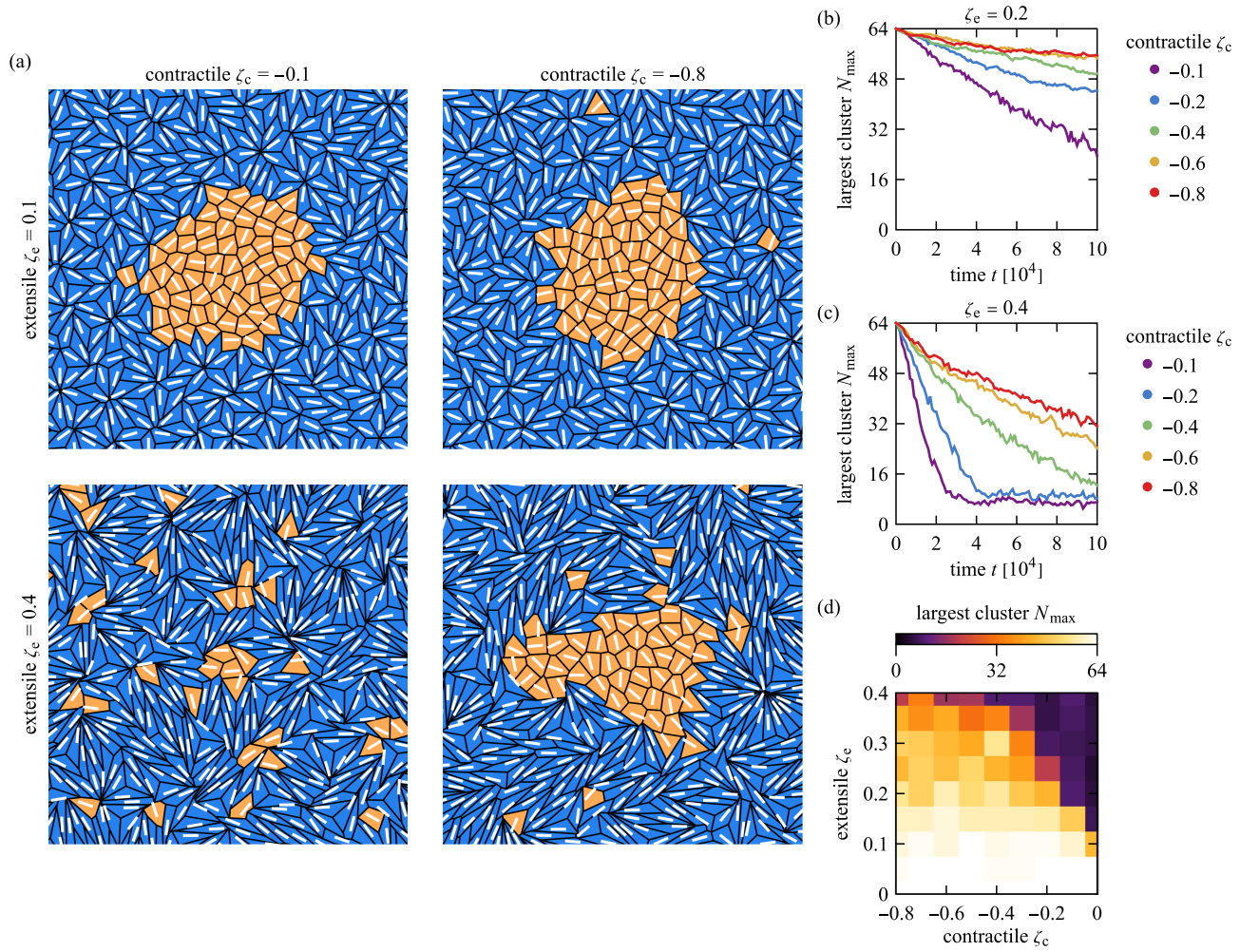

FIG. 3. (a) Largest connected cluster of contractile cells at $t = 5 \times 10^4$ starting from a contractile (orange) cluster of 64 cells surrounded by an extensile (blue) bulk, for different combinations of extensile and contractile activity. (b),(c) Size of the largest contractile cluster for different contractile activities ζ_c at $\zeta_e = 0.2$ (b) and $\zeta_e = 0.4$ (c); data averaged over 10 simulation runs at each set of parameters. (d) Size of the largest contractile cluster at $t = 10^5$ as a function of extensile and contractile activity. Each value corresponds to one simulation at that set of parameters. $k_P = 0.02$ and $p_0 = 3.95$ for all panels.

necessary to pull apart a pair of adjacent contractile cells in an otherwise passive tissue. This force increases approximately linearly with the magnitude of contractile activity. See Fig. S6 and Supplemental Material, Sec. IV [45], for details.

These observations suggest the following mechanism for phase separation: as in a purely extensile system, extensile activity induces chaotic flows that result in cell rearrangements. When contractile cells come into contact, they then tend to remain connected due to the contractile-activity-induced effective attraction. This tendency becomes more pronounced as the magnitude of contractile activity increases, whereas further increasing extensile activity hinders it, due to higher extensile activity inducing stronger chaotic flows which can then break apart connected contractile cells.

If there is no extensile activity in the first place, flows do not develop, preventing the necessary rearrangements for cell sorting. Thus this also explains why contractile-contractile and contractile-passive mixtures do not phase separate [Figs. S4(a) and S4(c) [45]]. However, extensile-extensile and extensile-passive mixtures still show some phase separation, which indicates that mechanisms such as differential diffusivity discussed above also play a role [Figs. S4(b) and S4(d) [45]], noting that a higher activity in a purely extensile system corresponds to a higher diffusion coefficient [Fig. S4(e) [45]].

For, e.g., the parameter set shown in Fig. 1(b), a system that starts out fully phase separated has a higher passive energy after the start of the simulation when compared to an initially mixed system. Moreover, as the mixed system phase separates at that set of parameters, its passive energy increases (Fig. S7 [45]). This indicates that the phase separation is not primarily driven by the passive contributions of the model. Note, however, that there are also parameter combinations where sorting is accompanied by a reduction of the passive energy. Lastly, there is a small

difference is cell areas between extensile and contractile cells [average area of 0.981 and 1.019, respectively, for the tissue in Fig. 1(b)]. While differences in cell area have been shown to lead to clone dispersion and tissue fluidization [47,48], they do not appear to be driving sorting here: a fivefold increase in area elasticity reduces the difference in area so that the mean value is 0.996 for extensile vs 1.004 for contractile cells but does not noticeably affect the extent of sorting (Fig. S8 and Supplemental Material, Sec. V [45]). Moreover, it has been shown that differences in cell area do not lead to demixing on large scales in a vertex model [32].

Discussion—We studied a mixture of extensile and contractile cells using an active nematic vertex model. For appropriate choices of activity, the cell mixture can fully separate, so that almost all extensile and almost all contractile cells each form a single contiguous region. More generally, the magnitude of the phase ordering at the end of the simulation depends monotonically on contractile activity with increasing magnitude of contractile activity leading to better (or equal) sorting. Conversely, the dependence on extensile activity is nonmonotonic, with an optimal extensile activity magnitude for phase separation at a given set of parameters (Fig. 1).

This behavior can be interpreted by noting that extensile cells in the mixture are more motile than contractile ones (Fig. 2). They tend to stir the mixture so that cells undergo neighbor exchange. Contractile cells that come into contact as a result then tend to remain in a connected cluster due to contractile activity resulting in an effective attraction between those cells (Fig. 3). If, however, the extensile cells are too active they are able to break up the clusters, hindering phase separation. Note that the cluster simulations shown in Fig. 3 are also pertinent to understanding the conditions for a connected group of cells to separate, which is relevant to, e.g., clone dispersion [47,48] and metastasis [49]. See Fig. S9 and Supplemental Material, Sec. VI [45], for cluster dispersion analysis under different activity combinations.

This Letter contributes to the recent theoretical literature concerning extensile-contractile phase separation in active nematics [23–25] in demonstrating strong sorting in the context of a model that resolves individual cells. The mechanism proposed here relies on effective attraction between contractile cells. It is, therefore, different from the phase separation in a mixture of two fluids with different nematic activities, which separate due to active anchoring at concentration gradients causing relative flows between the two fluids [23,25]. It would be interesting to analyze whether a continuum active nematic model extended to account for deformable nematogens [53], and therefore more closely resembling the active nematic vertex model, would lead to a similar phase separation mechanism as that discussed here.

Acknowledgments—We wish to thank Matej Krajnc for providing the initial version of the vertex model code and Saraswat Bhattacharyya, James N. Graham, Ioannis Hadjifrangiskou, Chaithanya K. V. S., Francesco Mori, and Rastko Sknepnek for many helpful discussions. We acknowledge support from the UK Engineering and Physical Sciences Research Council (Award No. EP/W023849/1) and ERC Advanced Grant ActBio (funded as UKRI Frontier Research Grant No. EP/Y033981/1).

[1] B. Dutagaci, G. Nawrocki, J. Goodluck, A. A. Ashkarran, C. G. Hoogstraten, L. J. Lapidus, and M. Feig, eLife **10**, e64004 (2021).
[2] S. F. G. Krens and C.-P. Heisenberg, Curr. Top. Dev. Biol. **95**, 189 (2011).
[3] A. Moscona and H. Moscona, J. Anat. **86**, 287 (1952).
[4] P. L. Townes and J. Holtfreter, J. Exp. Zool. **128**, 53 (1955).
[5] A. Gierer, S. Berking, H. Bode, C. N. David, K. Flick, G. Hansmann, H. Schaller, and E. Trenkner, Nat. New Biol. **239**, 98 (1972).
[6] O. Cochet-Escartin, T. T. Locke, W. H. Shi, R. E. Steele, and E.-M. S. Collins, Biophys. J. **113**, 2827 (2017).
[7] E. Batlle and D. G. Wilkinson, Cold Spring Harbor Perspect. Biol. **4**, a008227 (2012).
[8] S. Pawlizak, A. W. Fritsch, S. Grosser, D. Ahrens, T. Thalheim, S. Riedel, T. R. Kießling, L. Oswald, M. Zink, M. L. Manning, and J. A. Käs, New J. Phys. **17**, 083049 (2015).
[9] M. S. Steinberg, Science **141**, 401 (1963).
[10] R. A. Foty and M. S. Steinberg, Dev. Biol. **278**, 255 (2005).
[11] S. Ramaswamy, Annu. Rev. Condens. Matter Phys. **1**, 323 (2010).
[12] M. C. Marchetti, J. F. Joanny, S. Ramaswamy, T. B. Liverpool, J. Prost, M. Rao, and R. A. Simha, Rev. Mod. Phys. **85**, 1143 (2013).
[13] J. Tailleur and M. E. Cates, Phys. Rev. Lett. **100**, 218103 (2008).
[14] M. E. Cates and J. Tailleur, Annu. Rev. Condens. Matter Phys. **6**, 219 (2015).
[15] G. Gonnella, D. Marenduzzo, A. Suma, and A. Tiribocchi, C.R. Phys. **16**, 316 (2015).
[16] R. A. Simha and S. Ramaswamy, Phys. Rev. Lett. **89**, 058101 (2002).
[17] A. Doostmohammadi, J. Ignés-Mullol, J. M. Yeomans, and F. Sagués, Nat. Commun. **9**, 3246 (2018).
[18] T. B. Saw, A. Doostmohammadi, V. Nier, L. Kocgozlu, S. Thampi, Y. Toyama, P. Marcq, C. T. Lim, J. M. Yeomans, and B. Ladoux, Nature (London) **544**, 212 (2017).
[19] G. Duclos, S. Garcia, H. G. Yevick, and P. Silberzan, Soft Matter **10**, 2346 (2014).
[20] G. Duclos, C. Erlenkämper, J.-F. Joanny, and P. Silberzan, Nat. Phys. **13**, 58 (2017).
[21] D. Dell'Arciprete, M. L. Blow, A. T. Brown, F. D. C. Farrell, J. S. Lintuvuori, A. F. McVey, D. Marenduzzo, and W. C. K. Poon, Nat. Commun. **9**, 4190 (2018).
[22] L. Balasubramaniam, A. Doostmohammadi, T. B. Saw, G. H. N. Sankara Narayana, R. Mueller, T. Dang, M. Thomas, S. Gupta, S. Sonam, A. S. Yap, Y. Toyama,

R.-M. Mège, J. M. Yeomans, and B. Ladoux, Nat. Mater. **20**, 1156 (2021).
[23] S. Bhattacharyya and J. M. Yeomans, Phys. Rev. Lett. **130**, 238201 (2023).
[24] J. N. Graham, G. Zhang, and J. M. Yeomans, Soft Matter **20**, 2955 (2024).
[25] S. Bhattacharyya and J. M. Yeomans, Phys. Rev. E **110**, 024607 (2024).
[26] H. Honda and G. Eguchi, J. Theor. Biol. **84**, 575 (1980).
[27] R. Farhadifar, J.-C. Röper, B. Aigouy, S. Eaton, and F. Jülicher, Curr. Biol. **17**, 2095 (2007).
[28] A. G. Fletcher, M. Osterfield, R. E. Baker, and S. Y. Shvartsman, Biophys. J. **106**, 2291 (2014).
[29] S. Alt, P. Ganguly, and G. Salbreux, Phil. Trans. R. Soc. B **372**, 20150520 (2017).
[30] S.-Z. Lin, S. Ye, G.-K. Xu, B. Li, and X.-Q. Feng, Biophys. J. **115**, 1826 (2018).
[31] M. Krajnc, Soft Matter **16**, 3209 (2020).
[32] P. Sahu, D. M. Sussman, M. Rübsam, A. F. Mertz, V. Horsley, E. R. Dufresne, C. M. Niessen, M. C. Marchetti, M. L. Manning, and J. M. Schwarz, Soft Matter **16**, 3325 (2020).
[33] J. Comelles, Soumya S. S., L. Lu, E. Le Maout, S. Anvitha, G. Salbreux, F. Jülicher, M. M. Inamdar, and D. Riveline, eLife **10**, e57730 (2021).
[34] C. Duclut, J. Paijmans, M. M. Inamdar, C. D. Modes, and F. Jülicher, Eur. Phys. J. E **45**, 29 (2022).
[35] S. Sonam, L. Balasubramaniam, S.-Z. Lin, Y. M. Y. Ivan, I. Pi-Jaumà, C. Jebane, M. Karnat, Y. Toyama, P. Marcq, J. Prost, R.-M. Mège, J.-F. Rupprecht, and B. Ladoux, Nat. Phys. **19**, 132 (2023).
[36] S.-Z. Lin, M. Merkel, and J.-F. Rupprecht, Phys. Rev. Lett. **130**, 058202 (2023).
[37] J. Rozman, J. M. Yeomans, and R. Sknepnek, Phys. Rev. Lett. **131**, 228301 (2023).
[38] J. Rozman, Chaithanya K. V. S., J. M. Yeomans, and R. Sknepnek, arXiv:2312.11756.
[39] D. Bi, J. H. Lopez, J. M. Schwarz, and M. L. Manning, Nat. Phys. **11**, 1074 (2015).
[40] M. Merkel, K. Baumgarten, B. P. Tighe, and M. L. Manning, Proc. Natl. Acad. Sci. U.S.A. **116**, 6560 (2019).
[41] X. Wang, M. Merkel, L. B. Sutter, G. Erdemci-Tandogan, M. L. Manning, and K. E. Kasza, Proc. Natl. Acad. Sci. U.S.A. **117**, 13541 (2020).
[42] S. Tong, N. K. Singh, R. Sknepnek, and A. Košmrlj, PLoS Comput. Biol. **18**, e1010135 (2022).
[43] S. Tlili, J. Yin, J.-F. Rupprecht, M. A. Mendieta-Serrano, G. Weissbart, N. Verma, X. Teng, Y. Toyama, J. Prost, and T. E. Saunders, Proc. Natl. Acad. Sci. U.S.A. **116**, 25430 (2019).
[44] S.-Z. Lin, M. Merkel, and J.-F. Rupprecht, Eur. Phys. J. E **45**, 4 (2022).
[45] See Supplemental Material at http://link.aps.org/supplemental/10.1103/PhysRevLett.133.248401 for Figures S1–S10, caption for Movie S1, and additional background information and analysis, including Refs. [32,36,43,44,46–49].
[46] D. M. Sussman, Comput. Phys. Commun. **219**, 400 (2017).
[47] S. P. Ramanathan, M. Krajnc, and M. C. Gibson, Dev. Cell **51**, 49 (2019).
[48] L. Bocanegra-Moreno, A. Singh, E. Hannezo, M. Zagorski, and A. Kicheva, Nat. Phys. **19**, 1050 (2023).
[49] P. Friedl, J. Locker, E. Sahai, and J. E. Segall, Nat. Cell Biol. **14**, 777 (2012).
[50] M. Skamrahl, J. Schünemann, M. Mukenhirn, H. Pang, J. Gottwald, M. Jipp, M. Ferle, A. Rübeling, T. A. Oswald, A. Honigmann, and A. Janshoff, Proc. Natl. Acad. Sci. U.S.A. **120**, e2213186120 (2023).
[51] S. N. Weber, C. A. Weber, and E. Frey, Phys. Rev. Lett. **116**, 058301 (2016).
[52] E. McCarthy, R. K. Manna, O. Damavandi, and M. L. Manning, Phys. Rev. Lett. **132**, 098301 (2024).
[53] I. Hadjifrangiskou, L. J. Ruske, and J. M. Yeomans, Soft Matter **19**, 6664 (2023).